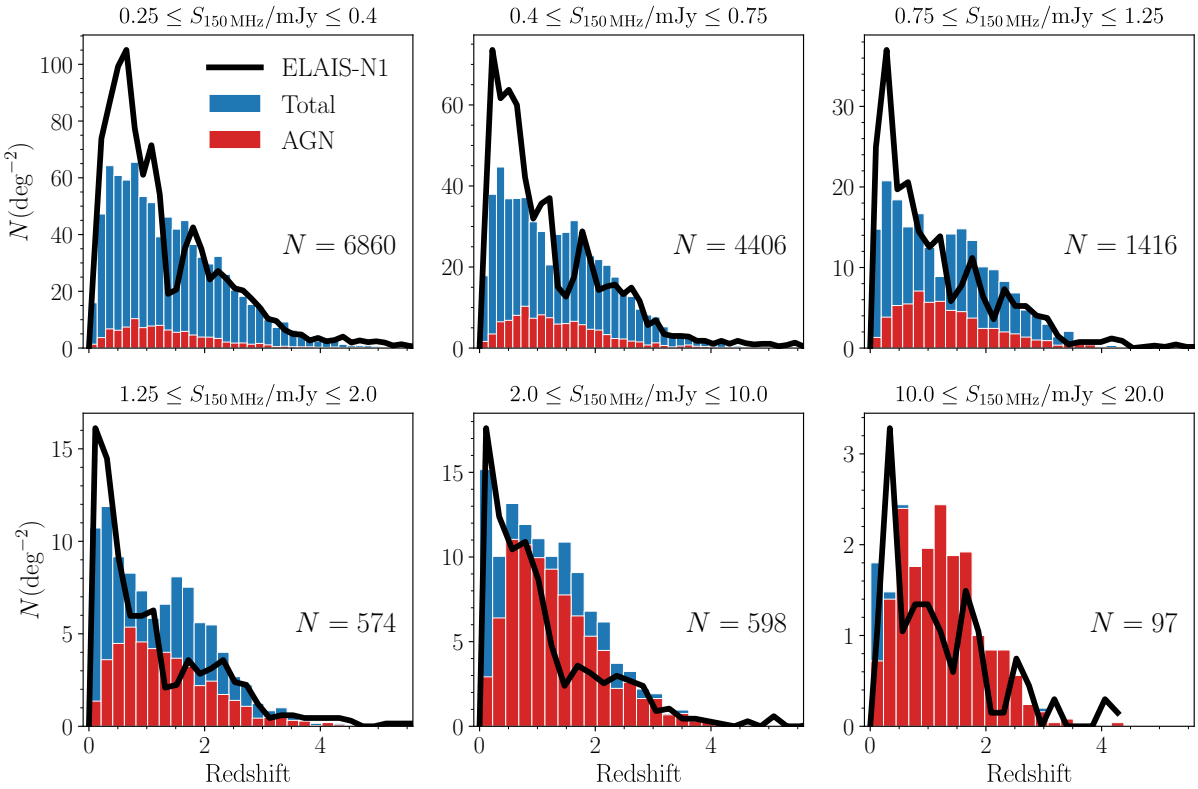

Fig. 11. Redshift distribution of the simulated sources in Bonaldi et al. (2019) catalog: the blue histogram corresponds to the total number of sources; the red histogram corresponds to the AGN component only. The solid black line shows the redshift distribution of the sources in the EN1 field. For a proper comparison the y-axis represents the source density in each catalog. Each panel corresponds to a different flux density bin, increasing *from left to right and from top to bottom*. Redshift bins range from $\Delta z = 0.14$ to $\Delta z = 0.22$ from the faintest to the brightest flux bin, i.e., they are larger than the estimated photometric redshift scatter by a factor 2−3 for AGN and by a factor ≥7 for galaxies. We caution that the EN1 redshift distributions are reliable only up to $z \sim 1.5$ for galaxies and up to $z \sim 4$ for AGN.

photometric and 9% spectroscopic, see Paper IV). 3% of the sources do not have redshift estimates, and are not included in the analysis. We believe the effect of neglecting these sources does not alter the main results of our analysis. Photometric redshifts can be considered robust up to $z = 1.5$ for galaxies ($\sigma_{\mathrm{NMAD}} = 1.48 \times \mathrm{median}(|\Delta z|/(1 + z_{\mathrm{spec}})) = 0.02$), and up to $z = 4$ for AGN ($\sigma_{\mathrm{NMAD}} = 0.064$; we refer to Paper IV for more details).

In Fig. 11 we show the redshift distributions of the sources in the EN1 field (solid black lines) for various flux density bins. These distributions are compared with the simulated distributions based on Bonaldi et al. (2019) evolutionary models (blue histogram bars). In the flux density bins spanning from 0.25 to 0.75 mJy we see a clear deficiency of the simulated sources, in agreement with the observed excess in the counts. This deficiency is mainly associated with sources at $z < 1$. The fact that the source counts' excess is observed in all of the LoTSS fields (see e.g., Fig. 8) seems to rule out the case this is due to cosmic variance. We cannot exclude however, that the clustering properties assumed in the simulation may play a role in producing the observed discrepancy[11]. At larger flux densities ($S \gtrsim 1$ mJy), we see an opposite trend, i.e., there is an excess of simulated sources with respect to observations. This is again consistent with the deficiency observed in our counts in the range 2−20 mJy. This excess is associated with intermediate redshift ($1 < z < 2$) sources, and appears to be mostly due to an excess of AGN in the simulated catalog, at least at flux densities larger than a few mJy. We note that both the source excess at sub-mJy fluxes and the AGN deficiency at the brightest fluxes are observed at redshifts where the involved populations (galaxies and AGN in the former, AGN only in the latter) have robust photometric redshift estimates.

[11] We note, however, that a similar discrepancy is observed when comparing EN1 to the wide tier of the Bonaldi et al. (2019) simulations, where clustering is not implemented.

7. Conclusions

In this paper, we have presented the source number counts derived from the LoTSS Deep Fields: the Lockman Hole (LH), the Boötes (Boo) and the Elais-N1 (EN1). With central rms noise levels of 22, 33, 17 μJy beam^{-1} the LH, Boo and EN1 fields are the deepest obtained so far at 150 MHz, allowing us to get unprecedented observational constraints to the shape of the source counts at 150 MHz sub-mJy flux densities. We compared the source counts derived from the LoTSS deep fields with other existing source-counts determinations from low- and high- frequency radio surveys, and state-of-the-art evolutionary models. Our counts are in broad agreement with those from the literature, and show the well known upturn at $\lesssim$1 mJy, which indicates the emergence of the star forming galaxy population. More interestingly, our counts show for the first time a very pronounced drop around $S \sim 2$ mJy, which results in a prominent 'bump' at sub-mJy flux densities. Such a 'drop and bump' feature was not observed in previous counts' determinations (neither at 150 MHz nor at higher frequency). While sample variance can play a role in explaining the observed discrepancies, we believe this is

mostly the result of a careful analysis aimed at deblending confused sources from the radio source catalogs (see Paper II). Our counts cannot be fully reproduced by any of the existing evolutionary models. From a qualitative comparison with Bonaldi et al. (2019) simulated catalogs, we find that the sub-mJy 'bump' appears to be associated with an excess of low-redshift ($z < 1$) galaxies and/or AGN, while the drop at mJy flux densities seems to be due to a deficiency of AGN at redshifts $1 < z < 2$. A more in-depth investigation of these preliminary results will be the subject of forthcoming papers, based on more comprehensive comparisons with models.

Acknowledgements. We thank the anonymous referee for constructive suggestions that allowed us to improve our draft. This paper is based (in part) on data obtained with the International LOFAR Telescope (ILT) under project code LC3_008. LOFAR (van Haarlem et al. 2013a) is the Low Frequency Array designed and constructed by ASTRON. It has observing, data processing, and data storage facilities in several countries, that are owned by various parties (each with their own funding sources), and that are collectively operated by the ILT foundation under a joint scientific policy. The ILT resources have benefitted from the following recent major funding sources: CNRS-INSU, Observatoire de Paris and Université d'Orléans, France; BMBF, MIWF-NRW, MPG, Germany; Science Foundation Ireland (SFI), Department of Business, Enterprise and Innovation (DBEI), Ireland; NWO, The Netherlands; The Science and Technology Facilities Council, UK ; Istituto Nazionale di Astrofisica (INAF), Italy. This paper is based on the data obtained with the International LOFAR Telescope (ILT). The Leiden LOFAR team acknowledge support from the ERC Advanced Investigator programme NewClusters 321271 and the VIDI research programme with project number 639.042.729, which is financed by the Netherlands Organisation for Scientific Research (NWO). A.D. acknowledges support by the BMBF Verbundforschung under the grant 05A17STA. The Jülich LOFAR Long Term Archive and the German LOFAR network are both coordinated and operated by the Jülich Supercomputing Centre (JSC), and computing resources on the supercomputer JUWELS at JSC were provided by the Gauss Centre for supercomputing e.V. (grant CHTB00) through the John von Neumann Institute for Computing (NIC). T.M.S. and D.J.S. acknowledge the Research Training Group 1620 'Models of Gravity', supported by Deutsche Forschungsgemeinschaft (DFG) and support of the German Federal Ministry for Science and Research BMBF-Verbundforschungsprojekt D-LOFAR IV (grant number 05A17PBA). P.N.B. is grateful for support from the UK STFC via grant ST/R000972/1. M.J.H. acknowledges support from the UK Science and Technology Facilities Council (ST/R000905/1). I.P. and M.B. acknowledge support from INAF under PRIN SKA/CTA "FORECaST" and PRIN MAIN STREAM "SAuROS" projects, as well as from the Ministero degli Affari Esteri e della Cooperazione Internazionale - Direzione Generale per la Promozione del Sistema Paese Progetto di Grande Rilevanza ZA18GR02. J.S. is grateful for support from the UK STFC via grant ST/R000972/1. M.J.J. acknowledges support from the UK Science and Technology Facilities Council [ST/N000919/1] and the Oxford Hintze Centre for Astrophysical Surveys which is funded through generous support from the Hintze Family Charitable Foundation. R.K. acknowledges support from the Science and Technology Facilities Council (STFC) through an STFC studentship via grant ST/R504737/1. W.L.W. acknowledges support from the ERC Advanced Investigator programme NewClusters 321271. W.L.W. also acknowledges support from the CAS-NWO programme for radio astronomy with project number 629.001.024, which is financed by the Netherlands Organisation for Scientific Research (NWO). K.L.E. acknowledges financial support from the Dutch Science Organization (NWO) through TOP grant 614.001.351. This research made use of APLpy, an open-source plotting package for Python hosted at `http://aplpy.github.com`.

References

Baldwin, J. E., Boysen, R. C., Hales, S. E. G., et al. 1985, MNRAS, 217, 717
Becker, R. H., White, R. L., & Helfand, D. J. 1995, ApJ, 450, 559
Bennett, A. S. 1962, MNRAS, 68, 163
Bonaldi, A., Bonato, M., Galluzzi, V., et al. 2019, MNRAS, 482, 2
Bonato, M., Negrello, M., Mancuso, C., et al. 2017, MNRAS, 469, 1912
Bonato, M., Prandoni, I., De Zotti, G., et al. 2021, MNRAS, 500, 22
Bondi, M., Ciliegi, P., Zamorani, G., et al. 2003, A&A, 403, 857
Bondi, M., Ciliegi, P., Schinnerer, E., et al. 2008, ApJ, 681, 1129
Bondi, M., Zamorani, G., Ciliegi, P., et al. 2018, A&A, 618, L8
Bonzini, M., Padovani, P., Mainieri, V., et al. 2013, MNRAS, 436, 3759
Bonzini, M., Mainieri, V., Padovani, P., et al. 2015, MNRAS, 453, 1079
Brunner, H., Cappelluti, N., Hasinger, G., et al. 2008, A&A, 479, 283
Calistro Rivera, G., Williams, W. L., Hardcastle, M. J., et al. 2017, MNRAS, 469, 3468
Chambers, K. C., Magnier, E. A., Metcalfe, N., et al. 2016, ArXiv e-prints [arXiv:1612.05560]
Condon, J. J., Cotton, W. D., Greisen, E. W., et al. 1998, AJ, 115, 1693
Condon, J. J., Cotton, W. D., Fomalont, E. B., et al. 2012, ApJ, 758, 23
Coppejans, R., Cseh, D., Williams, W. L., van Velzen, S., & Falcke, H. 2015, MNRAS, 450, 1477
Cotton, W. D., Condon, J. J., Kellermann, K. I., et al. 2018, ApJ, 856, 67
Croft, S., van Breugel, W., Brown, M. J. I., et al. 2008, AJ, 135, 1793
de Gasperin, F., Dijkema, T. J., Drabent, A., et al. 2019, A&A, 622, A5
Delvecchio, I., Smolčić, V., Zamorani, G., et al. 2017, A&A, 602, A3
de Vries, W. H., Morganti, R., Röttgering, H. J. A., et al. 2002, AJ, 123, 1784
Drabent, A., Hoeft, M., Mechev, A. P., et al. 2019, ArXiv e-prints [arXiv:1910.13835]
Duncan, K. J., Kondapally, R., Brown, M. J. I., et al. 2021, A&A, 648, A4 (LoTSS SI)
Eddington, A. S. 1913, MNRAS, 73, 359
Eddington, A. S. 1940, MNRAS, 100, 354
Edge, D. O., Shakeshaft, J. R., McAdam, W. B., Baldwin, J. E., & Archer, S. 1959, MNRAS, 68, 37
Eisenhardt, P. R., Stern, D., Brodwin, M., et al. 2004, ApJS, 154, 48
Fotopoulou, S., Salvato, M., Hasinger, G., et al. 2012, ApJS, 198, 1
Gehrels, N. 1986, ApJ, 303, 336
Gower, J. F. R., Scott, P. F., & Wills, D. 1967, MNRAS, 71, 49
Guidetti, D., Bondi, M., Prandoni, I., et al. 2017, MNRAS, 471, 210
Hales, C. A., Norris, R. P., Gaensler, B. M., et al. 2014a, MNRAS, 441, 2555
Hales, C. A., Norris, R. P., Gaensler, B. M., & Middelberg, E. 2014b, MNRAS, 440, 3113
Hartley, P., Jackson, N., Sluse, D., Stacey, H. R., & Vives-Arias, H. 2019, MNRAS, 485, 3009
Herrera Ruiz, N., Middelberg, E., Norris, R. P., & Maini, A. 2016, A&A, 589, L2
Herrera Ruiz, N., Middelberg, E., Deller, A., et al. 2017, A&A, 607, A132
Heywood, I., Jarvis, M. J., & Condon, J. J. 2013, MNRAS, 432, 2625
Hildebrandt, H., Choi, A., Heymans, C., et al. 2016, MNRAS, 463, 635
Hopkins, A. M., Afonso, J., Chan, B., et al. 2003, AJ, 125, 465
Hurley-Walker, N., Callingham, J. R., Hancock, P. J., et al. 2017, MNRAS, 464, 1146
Huynh, M. T., Jackson, C. A., Norris, R. P., & Prandoni, I. 2005, AJ, 130, 1373
Intema, H. T., van Weeren, R. J., Röttgering, H. J. A., & Lal, D. V. 2011, A&A, 535, A38
Intema, H. T., Jagannathan, P., Mooley, K. P., & Frail, D. A. 2017, A&A, 598, A78
Ishwara-Chandra, C. H., Sirothia, S. K., Wadadekar, Y., Pal, S., & Windhorst, R. 2010, MNRAS, 405, 436
Jannuzi, B. T., & Dey, A. 1999, ASP Conf. Ser., 191, 111
Kenter, A., Murray, S. S., Forman, W. R., et al. 2005, ApJS, 161, 9
Kondapally, R., Best, P. N., Hardcastle, M. J., et al. 2021, A&A, 648, A3 (LoTSS SI)
Lawrence, A., Warren, S. J., Almaini, O., et al. 2007, MNRAS, 379, 1599
Lockman, F. J., Jahoda, K., & McCammon, D. 1986, ApJ, 302, 432
Lonsdale, C. J., Smith, H. E., Rowan-Robinson, M., et al. 2003, PASP, 115, 897
Lonsdale, C. J., Cappallo, R. J., Morales, M. F., et al. 2009, IEEE Proc., 97, 1497
Mahony, E. K., Morganti, R., Prandoni, I., et al. 2016, MNRAS, 463, 2997
Maini, A., Prandoni, I., Norris, R. P., Giovannini, G., & Spitler, L. R. 2016, A&A, 589, L3
Mancuso, C., Lapi, A., Prandoni, I., et al. 2017, ApJ, 842, 95
Martin, C., Barlow, T., Barnhart, W., et al. 2003, Proc. SPIE, 4854, 336
Martin, D. C., Fanson, J., Schiminovich, D., et al. 2005, ApJ, 619, L1
Mauch, T., Murphy, T., Buttery, H. J., et al. 2003, MNRAS, 342, 1117
Mauduit, J.-C., Lacy, M., Farrah, D., et al. 2012, PASP, 124, 1135
Mechev, A. P., Plaat, A., Oonk, J. B. R., Intema, H. T., & Röttgering, H. J. A. 2018, Astron. Comput., 24, 117
Mohan, N., & Rafferty, D. 2015, Astrophysics Source Code Library [record ascl:1502.007]
Murphy, E. J., Momjian, E., Condon, J. J., et al. 2017, ApJ, 839, 35
Murray, S. S., Kenter, A., Forman, W. R., et al. 2005, ApJS, 161, 1
Muxlow, T. W. B., Richards, A. M. S., Garrington, S. T., et al. 2005, MNRAS, 358, 1159
Muzzin, A., Wilson, G., Yee, H. K. C., et al. 2009, ApJ, 698, 1934
Ocran, E. F., Taylor, A. R., Vaccari, M., & Green, D. A. 2017, MNRAS, 468, 1156

Ocran, E. F., Taylor, A. R., Vaccari, M., Ishwara-Chandra, C. H., & Prandoni, I. 2020, MNRAS, 491, 1127
Oliver, S. J., Bock, J., Altieri, B., et al. 2012, MNRAS, 424, 1614
Owen, F. N., Morrison, G. E., Klimek, M. D., & Greisen, E. W. 2009, AJ, 137, 4846
Padovani, P., Miller, N., Kellermann, K. I., et al. 2011, ApJ, 740, 20
Padovani, P., Bonzini, M., Kellermann, K. I., et al. 2015, MNRAS, 452, 1263
Pilkington, J. D. H., & Scott, J. F. 1965, MNRAS, 69, 183
Polletta, M. d. C., Wilkes, B. J., Siana, B., et al. 2006, ApJ, 642, 673
Prandoni, I., Gregorini, L., Parma, P., et al. 2000a, A&AS, 146, 31
Prandoni, I., Gregorini, L., Parma, P., et al. 2000b, A&AS, 146, 41
Prandoni, I., Gregorini, L., Parma, P., et al. 2001, A&A, 365, 392
Prandoni, I., Parma, P., Wieringa, M. H., et al. 2006, A&A, 457, 517
Prandoni, I., Guglielmino, G., Morganti, R., et al. 2018, MNRAS, 481, 4548
Retana-Montenegro, E., Röttgering, H. J. A., Shimwell, T. W., et al. 2018, A&A, 620, A74
Richards, E. A. 2000, ApJ, 533, 611
Röttgering, H., Afonso, J., Barthel, P., et al. 2011, JApA, 32, 557
Sabater, J., Best, P. N., Tasse, C., et al. 2021, A&A, 648, A2 (LoTSS SI)
Schinnerer, E., Carilli, C. L., Scoville, N. Z., et al. 2004, AJ, 128, 1974
Schinnerer, E., Smolčić, V., Carilli, C. L., et al. 2007, ApJS, 172, 46
Shimwell, T. W., Röttgering, H. J. A., Best, P. N., et al. 2017, A&A, 598, A104
Shimwell, T. W., Tasse, C., Hardcastle, M. J., et al. 2019, A&A, 622, A1
Siewert, T. M., Hale, C., Bhardwaj, N., et al. 2020, A&A, 643, A100
Sirothia, S. K., Saikia, D. J., Ishwara-Chandra, C. H., & Kantharia, N. G. 2009, MNRAS, 392, 1403
Smirnov, O. M., & Tasse, C. 2015, MNRAS, 449, 2668
Smolčić, V., Schinnerer, E., Scodeggio, M., et al. 2008, ApJS, 177, 14
Smolčić, V., Novak, M., Bondi, M., et al. 2017, A&A, 602, A1
Tasse, C. 2014, ArXiv e-prints [arXiv:1410.8706]
Tasse, C., Hugo, B., Mirmont, M., et al. 2018, A&A, 611, A87
Tasse, C., Shimwell, T., Hardcastle, M. J., et al. 2021, A&A, 648, A1 (LoTSS SI)
van Haarlem, M. P., Wise, M. W., Gunst, A. W., et al. 2013, A&A, 556, A2
van Weeren, R. J., Brunetti, G., Brüggen, M., et al. 2016, ApJ, 818, 204
Vernstrom, T., Scott, D., Wall, J. V., et al. 2016, MNRAS, 462, 2934
Wayth, R. B., Lenc, E., Bell, M. E., et al. 2015, PASA, 32, e025
White, R. L., Becker, R. H., Helfand, D. J., & Gregg, M. D. 1997, ApJ, 475, 479
White, S. V., Jarvis, M. J., Häußler, B., & Maddox, N. 2015, MNRAS, 448, 2665
White, S. V., Jarvis, M. J., Kalfountzou, E., et al. 2017, MNRAS, 468, 217
Whittam, I. H., Riley, J. M., Green, D. A., et al. 2013, MNRAS, 429, 2080
Williams, W. L., Intema, H. T., & Röttgering, H. J. A. 2013, A&A, 549, A55
Williams, W. L., van Weeren, R. J., Röttgering, H. J. A., et al. 2016, MNRAS, 460, 2385
Williams, W. L., Hardcastle, M. J., Best, P. N., et al. 2019, A&A, 622, A2
Wilman, R. J., Miller, L., Jarvis, M. J., et al. 2008, MNRAS, 388, 1335
Windhorst, R., Mathis, D., & Neuschaefer, L. 1990, ASP Conf. Ser., 10, 389

Appendix A: LoTSS Deep Fields - Counts' tables

Table A.1. 150 MHz normalized differential radio-source counts as derived from the Lockman Hole final catalogs.

$S_{\rm min}$	$S_{\rm max}$	ΔS	x	$N_{\rm S}$	$N^{+\sigma}_{-\sigma}$	Sys$^-$	Sys$^+$	c_1	c_2
0.25	0.35	0.10	0.30	6673	$42.35^{0.52}_{0.52}$	4.56	2.82	1.12	1.34
0.35	0.50	0.15	0.42	5314	$48.08^{0.67}_{0.66}$	1.38	2.73	1.01	1.10
0.50	0.71	0.21	0.59	3545	$51.21^{0.87}_{0.86}$	0.24	2.48	1.00	1.06
0.71	1.00	0.29	0.84	2077	$49.18^{1.10}_{1.08}$	0.02	2.09	1.00	1.04
1.00	1.41	0.41	1.19	1119	$43.55^{1.34}_{1.30}$	0.04	1.54	1.01	1.03
1.41	2.00	0.59	1.68	683	$44.29^{1.76}_{1.70}$	0.00	1.89	1.01	1.02
2.00	2.83	0.83	2.38	390	$42.01^{2.24}_{2.13}$	0.00	1.94	1.01	1.01
2.83	4.00	1.17	3.36	272	$49.19^{3.16}_{2.98}$	0.00	2.77	1.01	1.01
4.00	5.66	1.66	4.76	184	$55.86^{4.42}_{4.12}$	0.00	3.60	1.01	1.01
5.66	8.00	2.34	6.73	148	$75.45^{6.71}_{6.20}$	0.00	4.09	1.01	1.01
8.00	11.3	3.30	9.51	132	$113.1^{10.7}_{9.9}$	0.0	4.0	1.01	1.01
11.3	22.6	11.3	16.0	172	$158.4^{13.0}_{12.1}$	0.0	2.3	1.01	1.01
22.6	45.3	22.7	32.0	128	$333.2^{32.1}_{29.5}$	0.0	1.3	1.01	1.01
45.3	90.5	45.2	64.0	74	$543.7^{70.6}_{63.2}$	0.2	2.2	1.01	1.01
90.5	181	90.5	128	45	$935.1^{160.2}_{139.4}$	2.5	4.2	1.01	1.01
181	724	543	362	46	2144^{363}_{316}	3	15	1.01	1.01
724	2896	2172	1448	17	6335^{1909}_{1537}	18	86	1.00	1.00

Notes. Columns are as follows: $S_{\rm min}$ and $S_{\rm max}$ are the minimum and maximum flux densities (expressed in mJy), respectively; Δ denotes the flux density intervals; x is the geometric mean of $S_{\rm min}$ and $S_{\rm max}$; $N_{\rm S}$ is the number of sources in respective bins; N is the normalized source counts and σ is the Poissonian errors on the normalized counts; Sys$^+$ and Sys$^-$ are the systematic errors, accounting for different modeling of resolution and Eddington bias corrections (see Sects. 4 and 5 for more details); the correction factor c_1 represents the weighting applied to the counts to account for resolution and Eddington biases; the correction factor c_2 also includes the weighting due to the visibility function.

Table A.2. 150 MHz normalized differential radio-source counts as derived from the Boötes final catalogs.

$S_{\rm min}$	$S_{\rm max}$	ΔS	x	$N_{\rm S}$	$N^{+\sigma}_{-\sigma}$	Sys$^-$	Sys$^+$	c_1	c_2
0.35	0.50	0.15	0.42	3992	$46.96^{0.76}_{0.74}$	1.91	3.38	1.04	1.19
0.50	0.70	0.20	0.59	3066	$53.73^{0.99}_{0.97}$	0.23	3.39	1.02	1.08
0.70	1.00	0.30	0.84	1812	$51.33^{1.23}_{1.21}$	0.00	2.76	1.02	1.06
1.00	1.41	0.41	1.19	949	$44.17^{1.48}_{1.43}$	0.00	2.01	1.02	1.03
1.41	1.99	0.58	1.68	580	$44.64^{1.93}_{1.85}$	0.00	2.55	1.02	1.02
1.99	2.82	0.83	2.37	345	$44.35^{2.52}_{2.39}$	0.00	2.94	1.02	1.02
2.82	3.99	1.17	3.35	234	$50.83^{3.54}_{3.32}$	0.00	3.98	1.01	1.02
3.99	5.64	1.65	4.74	155	$56.20^{4.88}_{4.51}$	0.00	4.99	1.01	1.02
5.64	7.97	2.33	6.70	146	$88.87^{7.96}_{7.36}$	0.00	6.99	1.01	1.01
7.97	11.3	3.33	9.48	117	$119.8^{12.1}_{11.1}$	0.0	5.9	1.01	1.01
11.3	22.6	11.3	15.9	125	$137.4^{13.4}_{12.3}$	0.0	2.8	1.01	1.01
22.6	45.1	22.5	31.9	96	$298.1^{33.5}_{30.4}$	0.0	1.4	1.01	1.01
45.1	90.2	45.1	63.8	75	$657.5^{84.7}_{75.9}$	0.8	3.2	1.01	1.01
90.2	180	89.8	128	41	1018^{184}_{159}	6	6	1.01	1.01
180	722	542	361	27	1502^{345}_{289}	3	12	1.01	1.01
722	2886	2164	1443	11	4861^{1908}_{1466}	9	48	1.00	1.00

Notes. Parameters as in Table A.1.

Table A.3. 150 MHz normalized differential radio-source counts as derived from the ELAIS-N1 final catalogs.

$S_{\rm min}$	$S_{\rm max}$	ΔS	x	$N_{\rm S}$	$N^{+\sigma}_{-\sigma}$	Sys$^-$	Sys$^+$	c_1	c_2
0.18	0.26	0.08	0.22	7187	$38.85^{0.46}_{0.46}$	6.69	2.52	1.16	1.29
0.26	0.36	0.10	0.31	5340	$43.54^{0.60}_{0.60}$	2.11	2.33	1.02	1.08
0.36	0.51	0.15	0.43	3397	$44.84^{0.78}_{0.77}$	0.63	1.97	1.00	1.03
0.51	0.73	0.22	0.61	2081	$45.40^{1.02}_{1.00}$	0.02	1.72	1.00	1.01
0.73	1.03	0.30	0.86	1165	$42.58^{1.28}_{1.25}$	0.00	1.32	1.00	1.01
1.03	1.45	0.42	1.22	676	$41.18^{1.65}_{1.58}$	0.00	1.07	1.01	1.01
1.45	2.06	0.61	1.73	368	$37.59^{2.06}_{1.96}$	0.00	1.01	1.01	1.01
2.06	2.91	0.85	2.45	232	$39.83^{2.79}_{2.62}$	0.00	1.35	1.01	1.01
2.91	4.11	1.20	3.46	163	$47.00^{3.97}_{3.68}$	0.00	2.05	1.01	1.01
4.11	5.82	1.71	4.89	100	$48.44^{5.33}_{4.84}$	0.00	2.41	1.01	1.01
5.82	8.23	2.41	6.92	86	$69.90^{8.35}_{7.54}$	0.00	2.46	1.00	1.00
8.23	11.6	3.37	9.79	66	$90.85^{12.56}_{11.18}$	0.00	2.35	1.01	1.01
11.6	23.3	11.7	16.5	89	$130.7^{15.3}_{13.9}$	0.0	1.0	1.00	1.00
23.3	46.6	23.3	32.9	93	$385.9^{44.2}_{40.0}$	0.0	1.2	1.00	1.00
46.6	93.1	46.5	65.8	54	$634.4^{98.1}_{86.3}$	0.4	2.1	1.00	1.00
93.1	186	92.9	132	37	1230^{235}_{202}	3	5	1.00	1.00
186	745	559	372	17	1271^{383}_{308}	2	8	1.01	1.01
745	2979	2234	1489	5	2980^{1929}_{1333}	7	34	1.00	1.00

Notes. Parameters as in Table A.1.